Indian Journal of Chemical Technology
Vol. 30, March 2023, pp. 205-210
DOI: 10.56042/ijct.v30i2.63383

Development of enhanced 3D flower like Gd doped NiO (GNO) based LPG gas sensor

D Sengottaiyan*[,1,2] & Moorthi Pichumani[1]

[1]Department of Nanoscience and Technology, Sri Ramakrishna Engineering College, Coimbatore 641 022, Tamil Nadu, India

[2]Department of Physics, SNS College of Technology, Coimbatore 641 035, Tamil Nadu, India

E-mail: dsengottaiyan@gmail.com

Received 18 May 2022; accepted 2 February

The Liquefied Petroleum Gas (LPG) sensing properties of pure NiO and Gd doped NiO nanoparticles (Gd - 1%, 3%, and 5%) have been prepared by polyol method and student. The prepared nanoparticles have been characterized by X-ray diffraction (XRD), Field emission scanning electron microscopy (FESEM), Transmission electron microscopy (TEM), Ultraviolet-visible spectroscopy, X-ray Photoelectron spectroscopy to study the structural, morphological, optical properties and electronic state of the prepared nanoparticles. XRD reveals that NiO nanoparticles have average crystallite size of about 12 - 26 nm and 3D flower like morphology with 2 - 3 µm size was recorded and TEM images reveals the presence of quasi spherical particles with nanosheets of thickness about 20 - 30 nm range. Optical absorption is found to be in UV region and bandgap energy in the range 3 - 3.6 eV. XPS confirms the presence Ni^{2+}, Ni^{3+} ions, Gd^{3+} ions and presence of two oxygen species lattice oxygen and adsorbed oxygen. LPG sensing properties have been studied in detail for both pure NiO and GNO nanoparticles (1%, 3%, 5% Gd doped NiO) and it demonstrate that doped Gd enhance the sensitivity response LPG gas at operating temperature range 160°C to 260°C

Keywords: Gadolinium, LPG gas sensor, NiO, Rare earth

Liquefied Petroleum Gas (LPG) widely used in industries and domestic purposes across the world. The main constituents of LPG gas are propane and butane. Due to high inflammable nature of LPG gasa small leakage causes severe damage to the life and the properties. Hence, high selective and efficient LPG gas sensors are essential to avoid the damage[1-4]. Nanostructured metal oxide semiconductors are widely employed for the fabrication of gas sensors[5]. SnO_2[6], ZnO[7], α-Fe_2O_3[8] are n-type metal oxide semiconductors widely used for oxidation type of gases and p-type metal oxide semiconductorsNiO[9-12], CuO[13-15], CoO[16-17] widely used for sensing reducing gases. Among the above, NiO is p-type semiconducting oxide with wide bandgap energy of 3.0 – 3.6 eV[18]. NiO is highly stable metal oxide synthesized using hydrothermal[19-21], coprecipitation[22], solvothermal[23], microemulsion[24], thermal decomposition[25] methods. NiO has used for the detection xylene[26], acetone[27], ethanol[28], etc. But for the detection of LPG gas only following literatures found. From the literatures, NiO based LPG sensor fabricated and sensing response of 244 % for 2 Vol% reported by Gupta *etal*[29]and the same group doped NiO with Zn (1%, 2%, 3%) to detect LPG gas and reported 5.33% response, 42 s/31 s response/recovery time[30]. Sn doped NiO nanostructures were prepared by co-precipitation method and obtained 30.46% LPG detection for 3% Sn doped NiO for 2.0 vol% LPG[31]. The detection of LPG gas sensor in ppm level (< 100 ppm) detection with fast response and recovery rate is the market need. In this work, we have synthesized Gd doped NiO 3D flower like nanostructures by polyol method. The Gd doping concentration was varied between 0% - 5% (wt%) and LPG detection performed towards the concentration 5–100 ppm.

Experimental Section

All the chemicals used in the synthesis purchased from Merck and used without any further purification

Synthesis of pure NiO and Gd doped NiO (GNO) nanoparticles

Pure NiO and Gd doped NiO (GNO) nanoparticles were prepared by polyol process. 0.1 M concentration of Nickel (II) nitrate hexahydrate (Ni $(NO_3)_2.6H_2O$(99%)) added to the 30 mL of 1,2-propanediol in 50 mL beaker. To add the dopant, Gadolinium Nitrate Hexahydrate ($Gd(NO_3)_3 \cdot 6H_2O$

(98%)) was used as precursor and dopant concentration was varied from 1%, 3%, 5% (wt%). The above mixed solution added with 0.3 M urea as complexing agent. After stirring 30 min, solution become clear, green and was added to 50 mL teflon lined stainless steel autoclave and kept at 160°C for 12 h in hot air oven. After 12 h, autoclave was allowed to cool, and the Gd-$Ni(OH)_2$ was obtained. The obtained intermediate product was annealed at 400°C for 2h to prepare Gd doped NiO nanoparticles (GNO nanoparticles).

Characterization

Crystallographic features of the nanoparticles were characterized by X-ray diffractometer (D8 Advance Bruker) in the 2θ range 30°- 80° using CuKα radiation withwavelength 1.5406 Å. Morphological features of samples were recorded by Field emission scanning electron microscopy (FESEM SIGMA HV – Carl Zeiss with Bruker Quantax 200) and transmission electron microscopy (JEOL- JEM 2100 TEM). Oxidation state of Gd-doped NiO nanoparticles was identified using Kratos Analytical Axis Ultra DLD with Al Ka1 source with energy of 1.486 keV. The optical property of the samples was analyzed with JASCO- 570 UV–Visible - spectrophotometer in the range 200 – 800 nm.Pure NiO and GNO nanoparticles were pelletized (dia: 10 mm , thickness : 5 mm) for LPG gas sensing measurements. The pellets were kept inside a vacuum chamber where LPG gas was allowed through mass flow controller for concentration range 5–100 ppm at various operating temperatures 160-260°C. The measurements were done using Keithley 2612 digital source meter connected to a computer. To determine the gas sensor the following relation was used,

$$R_e(\%) = \frac{R_{g-R_a}}{R_a} \times 100\%$$

Here R_g and R_a are resistance of LPG gas and air respectively.

Results and Discussion

Structural properties

Figure 1 shows the XRD pattern of pure NiO and GNO nanoparticles. The observed diffraction patterns match with JCPDS card 04- 0835 correspond to the *fcc* crystal structure of NiO. No more diffraction peaks associated with the impurities like Gd_2O_3, Ni_2O, metallic Ni were detected indicating the purity of prepared nanoparticles. All the peaks of GNO nanoparticles were shifted towards a higher Bragg's angle, and the intensities of peaks were also reduced than the pure NiO. The manifestation of peak shift and reduced intensity was attributed to small crystallite size and micro strains, induced by the doping of Gd ions. The strains were induced due tothe difference in the ionic radius between Gd^{3+} (0.093 nm) and Ni^{2+}(0.069 nm)[32]. Inter-planner spacing (d_{hkl}), average crystallite (D) size, micro strain (ε)and lattice parameter (a) of both pure NiO and GNO nanoparticles were estimated using the relations,

$$d_{hkl} = \frac{n\lambda}{2\,Sin\theta}\ \text{nm} \quad \ldots (1)$$

$$D = \frac{k\lambda}{\beta Cos\theta}\ \text{nm} \quad \ldots (2)$$

$$\varepsilon = \frac{\beta\ Cot\theta}{4} \quad \ldots (3)$$

$$S = \frac{6}{\rho \times D} \quad \ldots (4)$$

Where d_{hkl} is Inter-planner spacing, n is order of diffraction, λ is wavelength of X-rays (λ = 1.54046 nm), θ is Bragg's diffraction angle, k is shape factor β is full width half maximum (FWHM) and ρ is bulk density of NiO (6.67 g/cm^3).

Table 1 gives the structural parameters estimated using the relations (1) to (4). It observed from that

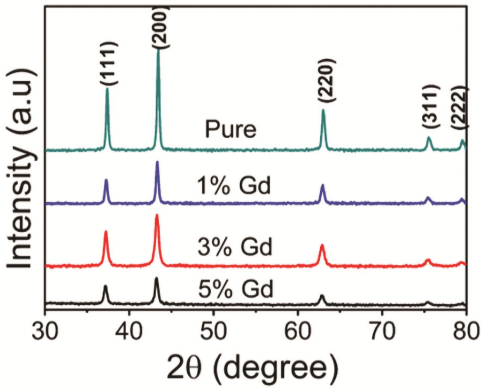

Fig. 1 — XRD pattern of pure NiO and GNONanoparticles

Table 1 — Structural Parameters of pure NiO and GNO nanoparticles.

Sample	d-spacing (nm)	Average crystallite size (nm)	Strain ε (× 10^{-4})	Specific surface area (m^2/g)
Pure NiO	0.2091	26.20	3.8210	34.33
1% GNO	0.2085	22.65	4.1128	39.71
3% GNO	0.2078	16.47	5.4492	54.61
5% GNO	0.2072	12.14	7.6321	74.09

average crystallite size reduces from 26.20 nm to 12.14 nm as Gd concentration increases 0 to 5% whereas specific surface area increases from 34.33 m^2/g to 74.09 m^2/g and strain also increases from 3.8210 to 7.6321 with increase in Gd concentration 0 to 5%, respectively.

Morphological studies

Figures 2 (a-c) shows the FESEM images of pure NiO, 1% and 5% GNO nanoparticles. FESEM images revealed a 3D flower-like morphology for both pure NiO and GNO nanoparticles. The size of each flower morphology was approximately 3 µm and it was observed that each flower was made of 2D nanosheets agglomerated with each other, and their thickness was found to be 40 - 50 nm. Doping Gd ions hasn't induced any considerable change up to 3% GNO, but at 5% GNO the nanosheets break and show the formation of holes with a reduction in size of the flower structure to approximately 2 µm. Fig. 2 (g-i) shows TEM images of pure NiO, 1% and 5% GNO nanoparticles. TEM images clearly depict that 2D nanosheets are the self-assembly of small nanoparticles with a size 28 nm and doping Gd (1% and 5%) reduced particle size to 15 nm and show the presence of sheet like morphology along with nano particulates. The SAED pattern shows 5 diffraction ring patterns, of which 3 bright patterns correspond to (111), (200), (220) planes and 2 low intense patterns correspond to (311), (222) planes, respectively. SAED results coincides with XRD diffraction patterns, which show the purity of the prepared nanoparticles. EDS spectrum (Fig. 2 (k-l)) displays the Ni, Gd and O elemental peaks.

Optical properties

Figure 3 (a) shows the optical absorption of pure NiO and GNO nanoparticles. Optical absorption shows a blue shift (lower wavelength shift) from 312 nm to 290 nm with increase in Gd concentration from 0 to 5% respectively. To determine the optical bandgap energy of pure NiO and GNO nanoparticles tau plot was drawn and shown in the Fig. 3(b). The optical bandgap energy increases 3.02 eV to 3.6 eV

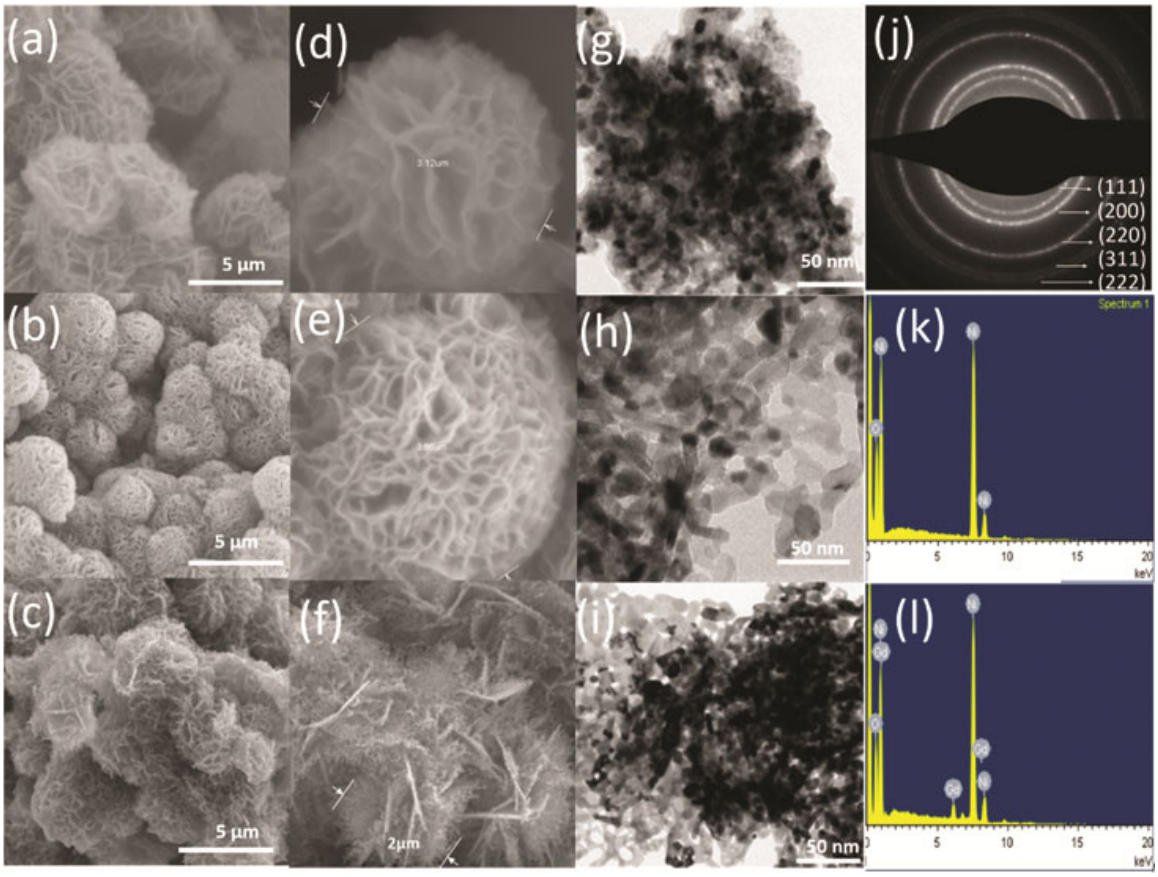

Fig. 2 — FESEM images of (a) pure NiO, (b) 1% GNO, (c) 5% GNO nanoparticles; Higher magnification FESEM images of (d) pure NiO (e) 1% GNO, (f) 5% GNO nanoparticles; TEM images of (g) pure NiO, (h) 1% GNO, (i) 5% GNO nanoparticles; (j) SAED pattern of 5% GNO; EDS spectra (k) pure NiO and (l) 5% GNO nanoparticles.

with increase in Gd concentration from 0 to 5% respectively. The blue shift in absorption and increase in bandgap energy is ascribed to decrease in the particle size of GNO nanoparticles.

X-ray Photoelectron spectroscopy

Figures 4 (a-d) show the full XPS spectra of GNO nanoparticles. Figure 4(b) shows the core level spectra of Ni show main peaks at 853.6 eV, 871.8 eV and 855.4 eV, 874 eV corresponds to Ni^{2+} and Ni^{3+}respectively. Besides, two satellite peaks were visible at 861.2 eV, 879.8 eV. Core level spectra of Gd (fig. 4(c))clearly reveals the presence single peak at 143 eV corresponding to Gd^{3+} ions and core level O1s spectra (Fig. 4(d)) shows two peaks at 529.5 eV and 531.2 eV belongs to lattice oxygen and surface adsorbed oxygen atoms.

LPG Gas Sensing properties

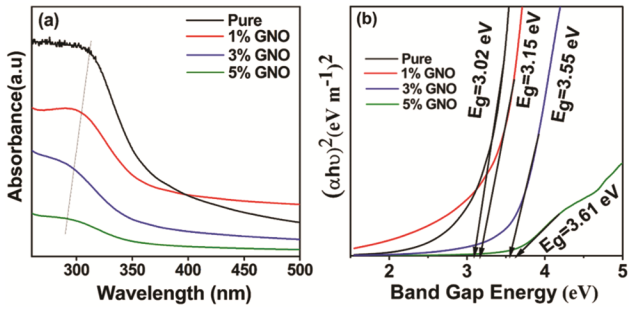

Fig. 3 — (a) Optical absorption of pure NiO and GNO nanoparticles and (b) Tau plot for determining band gap energy of pure NiO and GNO nanoparticles

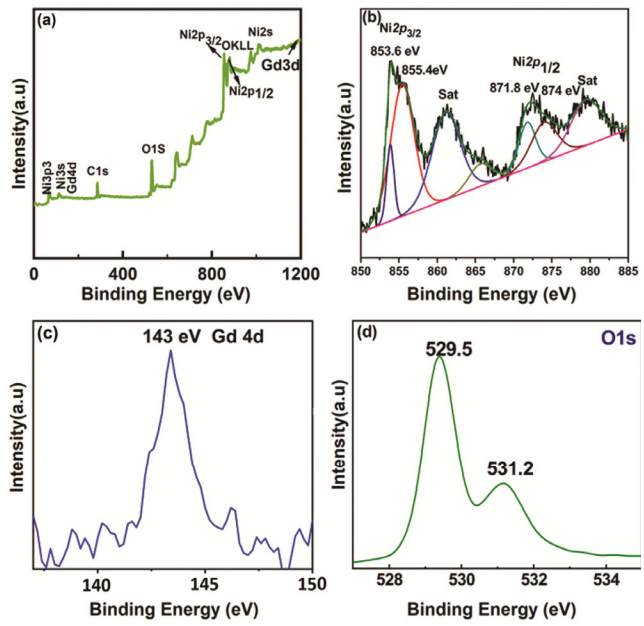

Fig. 4 — (a-d) XPS spectra of pure NiO and GNO nanoparticles

LPG gas sensing properties of pure and GNO nanoparticles were studied and shown in Figs 5 (a-e). Before exposing to LPG gas, sensors were maintained in the test chamber for 30 min to achieve equilibrium. The adsorption and desorption rates of the sensing materials are directly influenced by the operating temperature, which has a substantial effect on gas sensing performance. Initially, both pure and GNO nanoparticles were subjected to LPG gas at room temperature, which resulted in a low response. Hence, the prepared sensors are exposed to LPG gas at a 100-ppm concentration for operating temperature ranges between 160 and 260°C. Both pure and GNO nanoparticles exhibited improved performance at higher temperatures than the room temperature. Pure NiO nanoparticles exhibit a maximum response of 8.8 at 220°C, whereas 1, 3, and 5% GNO nanoparticles exhibit response values 10.7, 13.7, and 19.6 at 200°C, respectively (Fig. 5a). Optimum operating temperature of pure NiO was 220 ˚C where it reduces to 200°C after doping Gd^{3+} ions besides improved the sensitivity to LPG gas. The highest response value 19.6 was obtained by 5% GNO nanoparticles at 100 ppm LPG gas concentration at 200°C. Further increasing the operating temperature (above 200°C) the response of all the samples decreases gradually. Hence, the optimum operating temperature of the GNO-based LPG sensor is 200°C. This is because, below 160°C the interaction between the LPG gas molecules and adsorbed oxygen (O_{ads}) is feeble and, above 240°C, increase in the desorption rate of oxygen molecules (O_{Ds}). At an optimum operating temperature 200°C, both pure and GNO nanoparticles were exposed to different LPG concentrations from 100-500 ppm (Fig. 5b). The response valuesof all sensors increase with an increase in LPG concentration. When pure NiO nanoparticles were exposed to 100 ppm LPG gas at 200°C, the response value increases from 8.8 and reaches the highest value of 23 at 500 ppm. Similarly, 5% GNO nanoparticles also exhibited response value of 19.6 at 100 ppm and increased up to 42 at 500 ppm concentration. Dynamic performance of the gas sensors is determined by important parameters response and recovery times. These parameters of all the sensors are recorded at optimum operating temperature 200°C (Fig. 5c) towards100 ppm LPG gas concentration. Response /recovery times of pure NiO, 1, 3 and 5% GNO is 10 s /24 s, 20/40 s, 31/57 s and 36/75 s respectively. Both response/recovery time increases with doping concentration and can be attributed to the adsorption / desorption rate of gas molecules. Fig. 5d

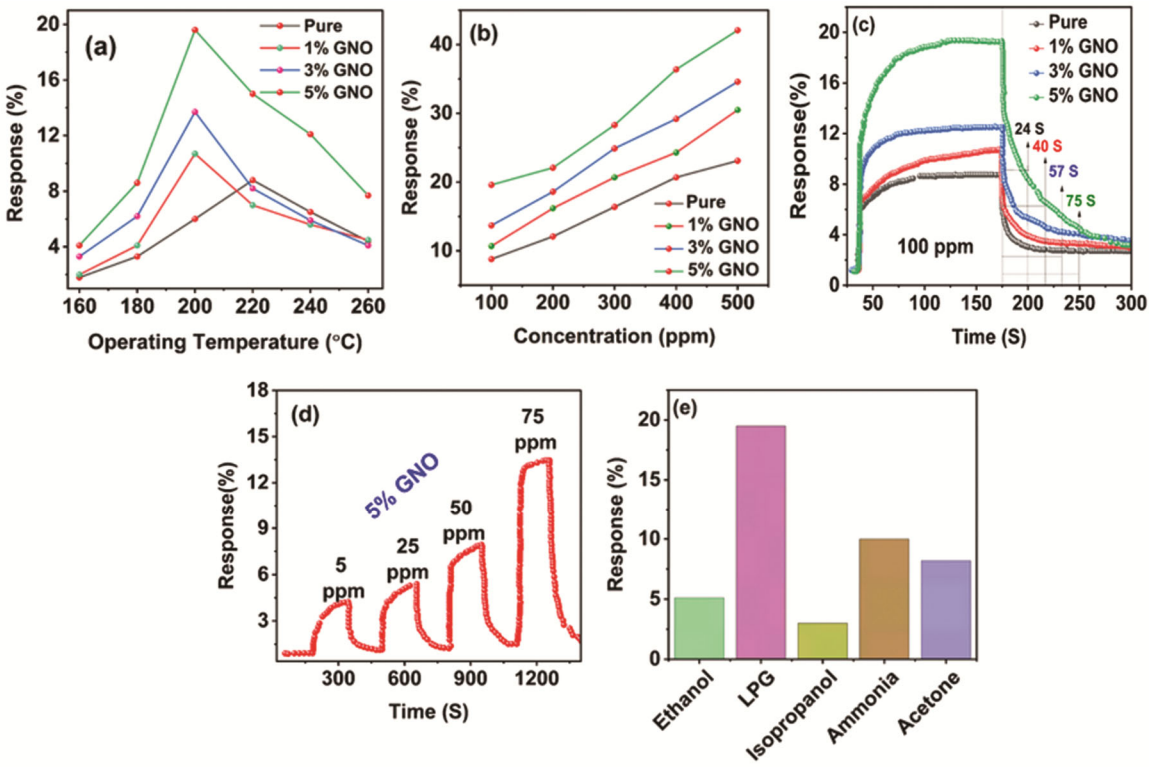

Fig. 5 — (a-e) LPG gas sensing properties of pure NiO and GNO nanoparticles

shows the transient response of 5% GNO nanoparticle sensors to different LPG concentrations, 5, 25, 50, and 75 ppm at 200°C. The response value increases from 4.29-13.63 as the LPG gas concentration rises. Selectivity is one of the important parameters to assess the performance of the gas sensor. From our study it is evidenced that 5% GNO based LPG sensor exhibited high response value. In this regard the same has been utilized for selectivity measurements. 5% GNO based sensors were exposed to different type of gases such as ethanol, LPG, isopropanol, acetone, ammonia at 200°C for 100 ppm. It is revealed (Fig. 5e) that 5% GNO sensor showing maximum response for LPG, which is 8 times than isopropanol.

The sensing mechanism of both pure NiO and GNO nanoparticles are surface driven phenomenon. The gas sensor's detecting process involves interactions between O_{ads} species and LPG gas on the material's surface. The sensor's resistance changes dramatically as it interacts with LPG gas molecules. In air, oxygen adsorption occurs until equilibrium is reached between chemisorption sites and oxygen molecules. O_{ads} molecules on the NiO sensor surface grab electrons from the conduction band, creating chemisorbed oxygen speciesO_2^- and $\bar{O}$ at different operating temperatures. This resulted in formation of hole-accumulation layer on the pure NiO or GNO sensor surface. When pure NiO or GNO sensors are exposed to LPG gas molecules, it will react with the chemisorbed oxygen species. During this process, the grabbed electrons are sent back to the conduction band and recombine with holes in valance band, thereby reducing the thickness of hole-accumulation layer led to the increase in electrical resistance of the sensor. The enhancement in sensitivity of GNO based sensors can be ascribed to doping of Gd^{3+} into Ni^{2+} lattice. The doping of Gd^{3+} ions reduced the holes concentration which subsequently raised the resistance of the sensor due to electronic compensation mechanism.

Conclusion

Pure and GNO nanoparticles were prepared by polyol method. 3D morphology with high specific surface area of 74.09 m^2/g, was achieved for 5% GNO nanoparticles. 5% GNO nanoparticle-based sensor show response of about 19.6 towards LPG gas for 100 ppm at operating temperature 200°C and can detect LPG upto 5 ppm concentration. Besides high response, sensors demonstrated 8 times high selectivity towards LPG than other gases

and recovery/response time of about 36/75 s, respectively.

References

1 Aishwary K, Nirmala R & Navamathavan R, *Sens Inter*, 2 (2021) 100091.
2 Singh A, Sikarwar S & Yadav B C, *Mater Res Express*, 8 (2021) 045013.
3 Kabure A A, Shirke B S, Mane S R, Garadkar K M, Sargar B M & Pakhare K S, *Appl Phys A*, 127 (2021) 711.
4 He Y, Sh X, Chen K & Yang X, *J Chen Nanomaterials*, 10 (2020) 727.
5 Gopi K K, Parne S, Pothukanuri N, Kathirvelu V, Gandi S & Joshi D, *Sens Actuat A: Phys*, 341 (2022) 113578.
6 Chaisitsak S, *Sensors*, 11 (2011) 7127.
7 Latyshev V M, Berestok T O, Opanasyuk A S, Kornyushchenko A S & Perekrestov V I, *Solid State Sci*, 67 (2017) 109.
8 Mirzaei A, Hashemi B & Janghorban K, *Mater Sci: Mater Electron*, 27 (2016) 3109.
9 Mokoena T P, Swart H C & Motaung D E, *J Alloys Comp*, 805 (2019) 267.
10 Zhang H, Chen W G, Li Y Q, Jin L F, Cui F & Song Z H, *Front Chem*, 6 (2018) 472.
11 Nie C, Zeng W & Li Y, *J Mater Sci: Mater Electron*, 30 (2019) 1794.
12 Wang J, Yang P & Wei X, *Nanoscale Res Lett*, 10 (2015) 119.
13 Wanga F, Li H, Yuana Z, Suna Y, Changa F, Denga H, Xiea L & Lic H, *RSC Adv*, 6 (2016) 79343.
14 Umar A, Ibrahim A A, Nakate U T, Albargi H, Alsaiari M A, Ahmed F, Alharthi F A, Alghamdi A A & Zaqri N A, *Chem Phy Lett*, 763 (2021)138204.
15 Hou L, Zhang C, Li L, Du C, Li X, Kang X F & Chen W, *Talanta*, 188 (2018) 41.
16 Tan J, Dun M, Li L & Huang X, *Mater Res Express*, 5 (2018) 045036.
17 Zhou T, Zhang T, Deng J, Zhang R, Lou Z & Wang L, *Sen Actu B: Chem*, 242 (2017) 369.
18 Hashem M, Saion E, Al-Hada N M, Kamari M H, Shaari A H, Talib Z A, Paiman S B & Kamarudeen M A, *Res Phy*, 6 (2016) 1024.
19 Cao S, Peng L, Han T, Liu B, Zhu D, Zhao C, Xu J, Tang Y, Wang J & He S, *Phys E: Low-dimen Sys Nanostruc*, 118 (2020) 113655.
20 Nguyen K, Hoa N D, Hung C M, Le D T T, Duy N V & Hieu N V, *RSC Adv*, 8 (2018) 19449.
21 Cuong N D, Tran T D, Nguyen Q T, Hai H V M, Hoa T T, Quang D T, Wantana K & Tran P D, *R Soc Open Sci*, 8 (2021) 202352.
22 Atul A K, Srivastava S K, Gupta A K & Srivastava N, *Braz J Phys*, 52 (2022) 2.
23 Brewster D A, Bian Y & Knowles K E, *Chem Mater*, 32 (2020) 2004.
24 Du Y, Wang W, Li X, Zhao J, Ma J, Liu Y & Lu G, *Mater Lett*, 68 (2012) 168.
25 Niasari M S, Mir N & Davar F, *Polyhedron*, 28 (2009) 1111.
26 Gao H, Wei D, Lin P, Liu C, Sun P, Shimanoe K, Yamazoe N & Lu G, *Sen Actu B: Chem*, 253 (2017) 1152.
27 Yang M, Lu J, Wang X, Zhang H, Chen F, Sun J, Yang J, Sun Y & Lu G, *Sen Actu B: Chem*, 313 (2020) 127965.
28 Bartolomé J, Taeño M, Casado R M, Maestre D & Cremades A, *App Surf Sci*, 579 (2022) 152134.
29 Gupta P, Kumar K, Pandey N K, Yadav B C & Saeed S H, *Appl Phys A*, 127 (2021) 289.
30 Gupta P, Pandey N K, Kumar K, Yadav B C, *Sen Actu A: Phys*, 319 (2021) 112484.
31 Gupta P, Kumar K, Saeed S H, Pandey N K, Verma V, Singh P & Yadav B C, *J Mater Res*, 37 (2022) 369.
32 Dash D & Sahu D, *IOP Conf. Series: Mater Sci Eng*, 1219 (2022) 012037.